

## Tuning Synthesis of Highly Active Nitrogen-doped Graphite and Determining the Optimal Structure from First-principles Calculations

Shujun Chao<sup>1,2</sup>, Zhansheng Lu<sup>3</sup>, Zhengyu Bai<sup>1</sup>, Qian Cui<sup>1</sup>, Jinli Qiao<sup>4</sup>, Zongxian Yang<sup>3</sup>, Lin Yang<sup>1,\*</sup>

<sup>1</sup> College of Chemistry and Chemical Engineering, Key Laboratory of Green Chemical Media and Reactions, Ministry of Education, Henan Normal University, Xinxiang 453007, P. R. China

<sup>2</sup> Department of Chemistry, Xinxiang Medical University, Xinxiang 453007, P. R. China

<sup>3</sup> College of Physics and Information Engineering, Henan Normal University, Xinxiang 453007, P. R. China

<sup>4</sup> College of Environmental Science and Engineering, Donghua University, Shanghai 201620, P. R. China

\*E-mail: [yanglin1819@163.com](mailto:yanglin1819@163.com)

Received: 15 April 2013 / Accepted: 12 May 2013 / Published: 1 June 2013

---

Metal-free, nitrogen-doped graphite catalysts were synthesized by the pyrolysis of polypyrrole/carbon black (CB) nanocomposites (P-PPy/CB). The catalysts were characterized by XPS, XRD and FESEM. The results of XPS showed that nitrogen atoms had been embedded in the graphitic carbon after pyrolysis and the effective conversion ratio of pyrrolic N to pyridinic N and graphitic N can be changed by altering the initial pyrrole and CB weight ratios. By comparison, P800-3:1 (the weight ratio of polypyrrole to CB 3:1 at 800 °C) showed the highest conversion rate of nitrogen. Electrochemical tests also indicated P800-3:1 had the highest activity for oxygen reduction via a four-electron pathway. Based on the experimental results, the optimal structure of the N doped graphite was proposed from first-principles calculations, as well as the details of the O<sub>2</sub> dissociation in atomic and electronic level. It was found that the carbon dimer in the N-doped center and other carbon atoms around the N doping act together as an electron reservoir in donating electrons for the O<sub>2</sub> adsorption and the cleavage of the O-O bond. The dissociation of O<sub>2</sub> on the N doped graphite to form two O<sup>-</sup> only needed to cross the very low energy barrier, which was in line with the high activity for the oxygen reduction reaction (ORR). These results indicate that P800-3:1 is a promising catalyst for ORR.

---

**Keywords:** Oxygen reduction; nitrogen-doped graphite; metal-free catalyst; polypyrrole; first-principles calculations

## 1. INTRODUCTION

Fuel cells are efficient, environmentally friendly energy conversion devices for power generation. However, the major obstacle in the energy-conversion efficiency of fuel cells is attributed to the slow kinetics of cathodic oxygen reduction reaction (ORR). Until now, the most practical electrocatalyst for the ORR is still Pt and Pt-based binary, ternary or quaternary metal alloys [1-4]. But, their high costs, limited abundance and poor durability have become major obstacles to the widespread commercialization of fuel cells. In recent years, there have been significant efforts to develop new non-noble metal [5, 6], metal-free catalysts [7, 8] in order to improve the performance and reduce the costs of the ORR electrocatalysts. Consequently, metal-free catalysts, especially heteroatom (such as phosphorous [9], sulfur [10], boron [11], the most important nitrogen)-doped carbon materials have attracted much interest because their high electrocatalytic activity towards the ORR, long-term stability and more tolerant to methanol than the commercial Pt-C electrocatalysts.

The nitrogen-doped carbon materials such as carbon nanotubes [12, 13], carbon xerogel [14], carbon microspheres [15] and graphene [16, 17] synthesized by different methods have been studied. From the experimental results, it is concluded that the type of the nitrogen species such as pyrrolic, pyridinic and oxidized nitrogen, particularly graphitic nitrogen [12, 18] have been claimed to play an important role in the improvement of the ORR activities. The schematic representations of N-doped graphene [19, 20] and N-doped CNTs [21] have been reported. However, the questions concerning whether the schematic representation can represent the most likely structure, namely whether it is the most favorable structure to the adsorption and dissociation of oxygen molecules are not mentioned. Therefore, the optimal structure to the adsorption and dissociation of oxygen molecules in the ORR among different pyrrolic, pyridinic and graphitic nitrogen need to be studied further.

Herein, the most favorable structure of the completely metal-free, nitrogen-doped graphite (NG) has been proposed from experimental results in conjunction with first-principles calculations based on DFT (Density Functional Theory). First-principles calculations are a powerful tool for computational structure and characterization. According to several key terms based on the experimental investigations, a dozen of the possible structures are firstly picked out from all of the amorphous structures of the NG. After that, first-principles energy calculations are used to compare energies for all possible structures in order to propose the most preferable structure of the synthesized NG.

Moreover, pyrrole was used as a raw material. The reasons are as follows: firstly, pyrrole has high initial nitrogen content; secondly, the type of nitrogen species can transform from pyrrolic N into pyridinic N and graphitic N by the thermal treatment of PPy which are the key to improve the electrocatalytic activity of ORR. Based on the above reasons, nitrogen-doped graphite catalysts were obtained by the thermal treatment PPy/CB via in situ chemical oxidative polymerization pyrrole from the surfaces of CB nanoparticles. The effects of pyrrole to CB weight ratios and the pyrolysis temperature on their ORR performance were investigated. Finally, P800-3:1 displayed the best electrocatalytic activity towards the ORR as compared to other synthetic catalysts because it could maximally convert pyrrolic N to pyridinic N and graphitic N.

## 2. EXPERIMENTAL AND THEORETICAL METHODES

### 2.1. DFT calculations

Periodic DFT calculations were performed by the Vienna Ab-initio Simulation Package (VASP). The exchange-correlation interactions were treated with the Perdew, Burke, and Ernzerhof (PBE) functional [22-24]. The electron-ion interactions were treated using the projector augmented wave (PAW) method [25]. Altogether 4 electrons were treated as valence electrons for C ( $2s^2 2p^2$ ), 5 electrons for N ( $2s^2 2p^3$ ), 6 electrons for O ( $2s^2 2p^4$ ), 1 electron for H ( $1s^1$ ). The wave functions were expanded in plane waves with a cut off energy of 500 eV. The Brillouin zone was sampled with a  $2 \times 3 \times 1$  k point centered at  $\Gamma$  for structure optimization [26]. The graphene layer and the adsorbates were free to relax until the self-consistent forces reached  $0.02 \text{ eV/\AA}$ .

The electronic structure and bonding features were analyzed by means of the Bader-type atomic charges and the electron localization functions (ELF) [27, 28]. ELF plots provided a measure of electron localization in space (e.g., as in a covalent bond) and would help to characterize the nature of the interaction between the adsorbed  $\text{O}_2$  and N doped graphite.

The Bader's "atoms in molecules" theory was used to assign charges to atoms and fragments. These charges provided useful clues to how the charge transfers between different atoms or fragments. One major issue with the normal charge density from the VASP code was that they only contain the valance charge density, which would give an unreal charge transfer of N dopant by Bader charge analysis in the N-doped graphene systems. Although the energetic properties of the N-doped graphene systems were not affected by this miscounting charge transfer, which was a necessary for the mechanisms of ORR. Considering this point, the core charge had been included for Bader charge analysis in the current study, by which a real charge transfer could be obtained.

### 2.2. Catalysts synthesis

#### 2.2.1 Synthesis of PPy/CB (the weight ratio 3:1) nanocomposites

In a typical synthesis procedure, carbon black (Vulcan®XC-72) (0.1 g), 30 mL of 36% acetic acid was dispersed in 120 mL of ethanol aqueous solution (volume ratio = 1:1) by ultrasonic dispersion for 30 min. 0.3 g pyrrole monomer in 10 mL ethanol was added into the above suspension and stirred for 30 min. Then, 20 mL 1 M  $(\text{NH}_4)_2\text{S}_2\text{O}_8$  was added slowly into the suspension with constant stirring for 12 h at  $50 \text{ }^\circ\text{C}$ . After the completion of the reaction, the resulting PPy/CB powder was filtered and rinsed with double-distilled water and absolute ethanol until the pH of the filtrate solution was neutral. The obtained black powder was dried at  $40 \text{ }^\circ\text{C}$  for 12 h.

The other weight ratios of PPy/CB nanocomposites were synthesized by changing the amount of 36% acetic acid and 1 M  $(\text{NH}_4)_2\text{S}_2\text{O}_8$ .

### 2.2.2 Pyrolysis of PPy/CB nanocomposites

The resulting powder was pyrolyzed at 400, 600, 800 or 900 °C for 1 h under N<sub>2</sub> atmosphere. After that, the catalyst was obtained as black powder.

### 2.3. Physical characterization

X-ray diffraction (XRD) analysis was performed using a D/max-2200/PC X-ray diffractometer with Cu K $\alpha$  radiation source. X-ray photoelectron spectroscopic (XPS) measurements were performed on an AXIS Ultra instrument using a monochromic Al X-ray source. The morphology of the catalyst was characterized by field emission scanning electron microscopy (FESEM, JSM 6701F) operating at 5.0 kV. BET surface area was determined at 77K on a Micrometrics ASAP 2020 analyzer.

### 2.4. Electrochemical preparation

The procedures of glass carbon electrodes (3.0 mm in diameter for the examination in the cyclic voltammetry, 4.0 mm in diameter for the examination in the linear sweep voltammetry) pretreatment were as follows: prior to use, the electrodes were polished mechanically with  $\gamma$ -aluminite powder under an abrasive paper to obtain a mirror-like surface, washed with DD water and absolute ethanol and allowed to dry in air. Briefly, the working electrode was prepared as follows: 4 mg catalyst was added into 1 mL ethanol and 40  $\mu$ L of 5 wt% perfluorosulfonic acid (PFSA), and ultrasonically mixed for 10 min to obtain a homogeneous ink. Then, 10  $\mu$ L and 18  $\mu$ L ink was respectively dispersed on glassy carbon electrode (3.0 mm and 4.0 mm o.d.) and dried at room temperature. The catalyst loading on a glassy carbon electrode was 544.8  $\mu$ g cm<sup>-2</sup>. For comparison, the commercial Pt-C (20%) modified electrodes were prepared in the same way.

### 2.5. Electrochemical measurements

Cyclic voltammetry (CV) measurements were carried out in a three electrode cell by using Solartron 1287 electrochemical test system (Solartron Analytical, England). A glassy carbon electrode (3.0 mm or 4.0 mm o.d.) coated with catalyst was used as the working electrode, a platinum foil (1 cm<sup>2</sup>) as the counter-electrode, and saturated calomel electrode (SCE) as the reference. All measured potentials were converted into the values referring to a standard hydrogen electrode (SHE). 0.1 M KOH was used as the electrolyte in all experiments. Before every electrochemical measurement, O<sub>2</sub> was then bubbled for 1 h to achieve the electrolyte solution saturated. The cyclic voltammograms (CVs) were recorded by the potential range from -0.76 to + 0.44 V with the scan rate of 50 mV s<sup>-1</sup>. RDE measurements were carried out on a CHI 660D potentiostat equipping with a model 616 RDE (Princeton Applied Research), and were recorded at different rotating speeds from 400 to 2500 rpm with a scan rate of 10 mV s<sup>-1</sup>. All electrochemical experiments were performed at 25  $\pm$  1 °C.

### 3. RESULTS AND DISCUSSION

#### 3.1. Structure analysis

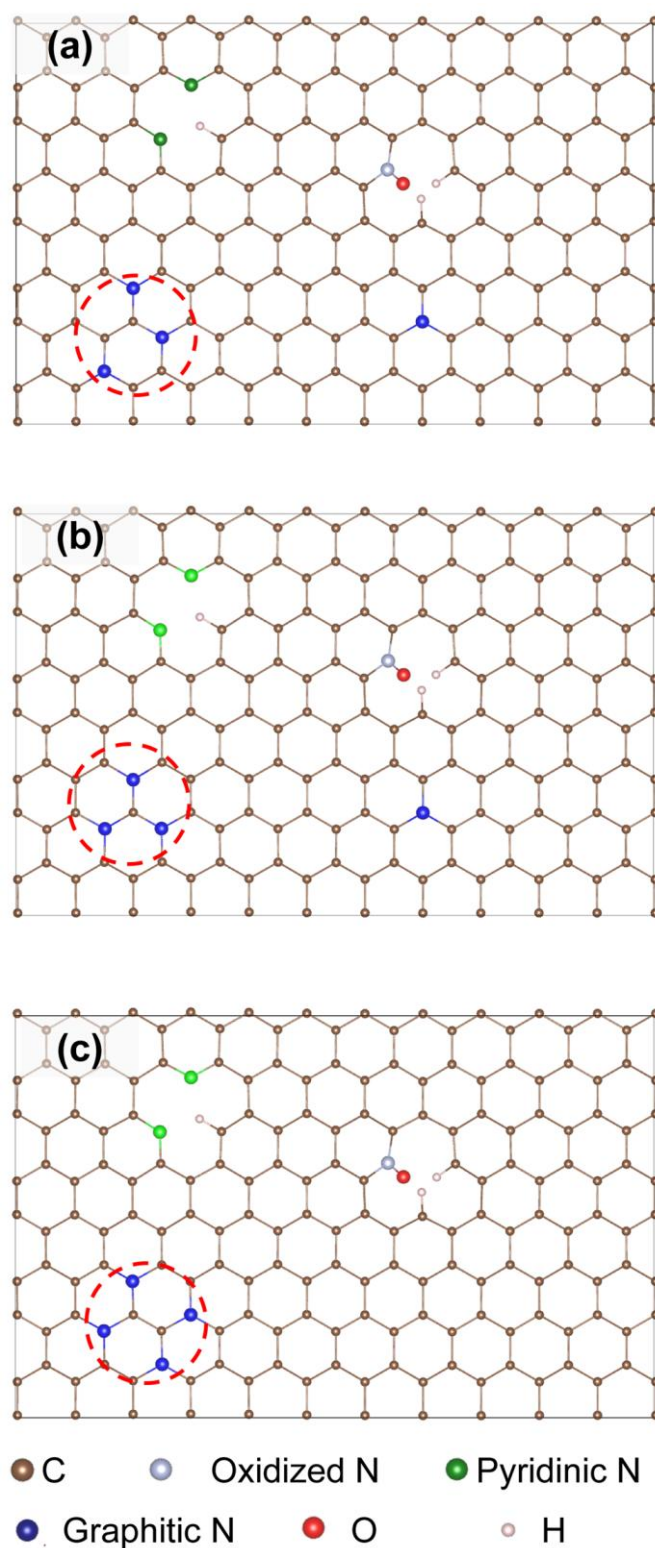


**Figure 1.** The model structures with various N doped configurations. The dashed red rings highlight the graphitic N doping (cluster). (a) a dopant cluster with three N dopants around a C dimer; (b) three N dopants around a sole C atom; (c) four N dopants around a C dimer.

The NG was prepared by a two-step method which included the synthesis of PPy/CB nanocomposites and high temperature treatment of the synthesized samples. PPy/CB nanocomposites were first synthesized via in situ chemical oxidative polymerization of pyrrole on the surface of CB; the NG was acquired by the pyrolysis of PPy/CB nanocomposites at 800 °C under N<sub>2</sub> atmosphere. In order to find the most appropriate proportion of pyrrole to carbon black and the pyrolysis temperature, different pyrrole to CB weight ratios 1:2, 1:1, 3:1 and 5:1 were investigated, and selected one with 3:1 was pyrolyzed under nitrogen atmosphere at 400 °C, 600 °C, 800 °C and 900 °C, respectively. Through the following electrochemical measurements, P800-3:1 was determined to show the highest electrocatalytic activity for the ORR among the synthesized catalysts. Therefore, 3:1 was considered as the main object of study.

The optimal structures of the synthesized NG with pyrrole to CB weight ratio 3:1 were proposed based on experimental results in conjunction with first-principles energetics calculations according to the following terms: 1) The highest catalytic activity was investigated by electrochemical measurements; 2) The element percentages of the C (90.16%), N (5.21%) and O (4.63%) were obtained from XPS and elemental analysis; 3) The atomic concentrations of pyridinic N (29.60%), graphitic N (53.72%) and oxidized N (16.68%) were concluded from XPS; 4) Nitrogen doping cluster with three or four nitrogen atoms was firstly considered because sole nitrogen doping could not be the good catalyst for ORR [29, 30].

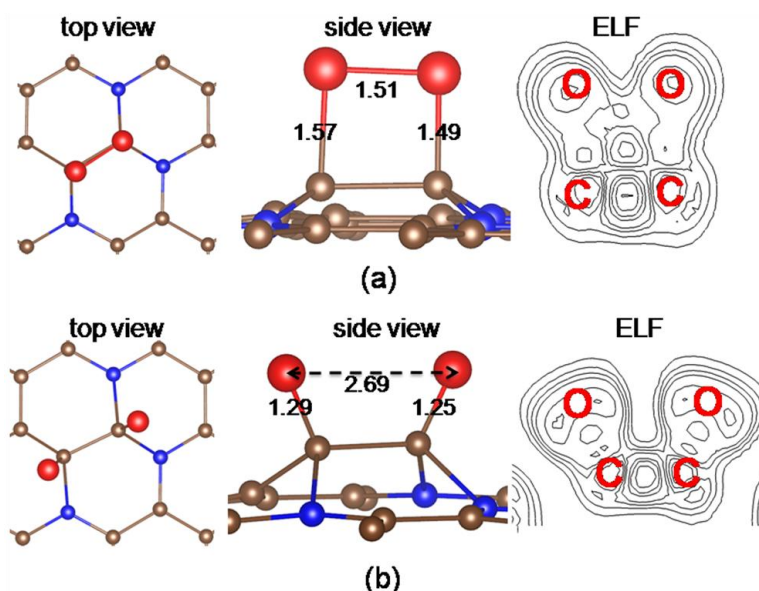


**Figure 2.** The two stable configurations for O<sub>2</sub> adsorption on NG, "structure I" (a) and "structure II" (b); "top view": the top view of the final structure; "side view": the side view of the final structure; "ELF": the contours for the electron localization function (ELF) in a vertical plane passing through two C-O bond and O adatoms, starting from 0.1 and increase successively by 0.1.

Based on those terms, several possible structures of NG are modeled with different kind of N dopant clusters (shown in Fig. 1), and the stability of the possible structures is checked by first-

principles energetics calculations. Fig. 1a presents the N dopants cluster with three N dopants around a C dimer. The N dopants cluster with three N dopants around one sole C atom is shown in Fig. 1b. And Fig. 1c illustrates the N dopants cluster with four N dopants around a C dimer. The NG with a nitrogen-doped cluster with three N dopants (Fig. 1a) would be the most stable model from the first-principles energetics calculation, which may be the most possible structure of the NG from our experimental synthesis. The structures presented in Fig. 1b and c are higher in energy by 0.61 and 0.53 eV (less stable) than that of the Fig. 1a, respectively.

The adsorption property of the  $O_2$  on the NG is investigated by first-principles from several different initial adsorption configurations. There are two stable configurations for  $O_2$  adsorption on the NG which are shown in Fig. 2a and b, respectively. In Fig. 2a,  $O_2$  is stable in the side-on configurations with the adsorption energy of 0.70 eV, marked as "structure I". Upon adsorption, the O-O bond is elongated from 1.29 Å (for a gas  $O_2$  molecule) to 1.51 Å and formed two new C-O bonds. The ELF maps confirm the covalent bond between the O-O and the new formed C-O bonds. Moreover, the adsorbed  $O_2$  is negative charged by 0.84 |e|, resulting in the formation of the  $O_2^-$  in "structure I".

The most stable structure, marked as "structure II", has the adsorption energy of 1.87 eV and a much elongated O-O bond (2.69 Å). The cleavage of the O-O bond is confirmed by the ELF maps (Fig. 2b). The Bader-type charge analysis shows that the two O atoms are both negatively charged by  $\sim 1.0$  |e|, indicating the formation of  $O^-$  in "structure II".

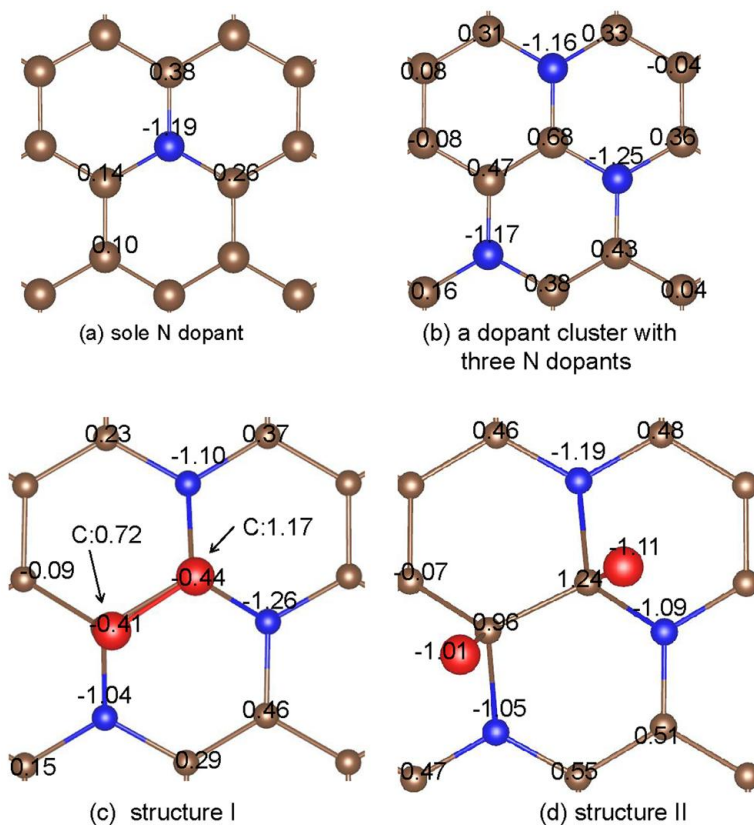


**Figure 3.** Bader-type charge of the selected atoms relative to their neutral atomic charge: (a) sole N dopant; (b) a dopant cluster with three N dopants around a C dimer; (c) "structure I"; (d) "structure II".

The Bader-type charge analysis of the selected atoms around N is used to further understand the nitrogen doping effect for the ORR. The calculated charges of atoms around N of the NG with and without O<sub>2</sub> adsorption are presented in Fig. 3. Upon the sole N atom doping, the two C atoms around the sole N dopant are positively charged by 0.38 and 0.26 |e| relative to the neutral atomic charge, respectively (Fig. 3a). This is due to the higher electronegativity of nitrogen than that of the carbon. Moreover, the two C atoms of the carbon dimer in the center of the N dopants cluster are positively charged by 0.47 and 0.68 |e|, respectively, resulting in the carbon dimer positively charged by 1.15 |e| (Fig. 3b), which is the most preferred O<sub>2</sub> adsorb site and the active center for the ORR, as presented above. Comparing Fig. 3c with Fig. 3b, it is found that the carbon dimer is further positively charged from 1.15 |e| to 1.89 |e| upon O<sub>2</sub> adsorption, indicating that the charge (0.85 |e|) transferred from the support to the adsorbed O<sub>2</sub><sup>-</sup> fragment is mainly from the carbon dimer in the center of the N dopant. Upon the cleavage of the O-O bond (Fig. 3d), the O<sub>2</sub><sup>-</sup> gets 1.27 |e| from the support to form two O<sup>-</sup>. The charge (1.27 |e|) is mainly from the carbon dimer in the center of the N-doped cluster (0.31 |e|) and the four carbon atoms near the N dopants (~ 0.92 |e| totally).

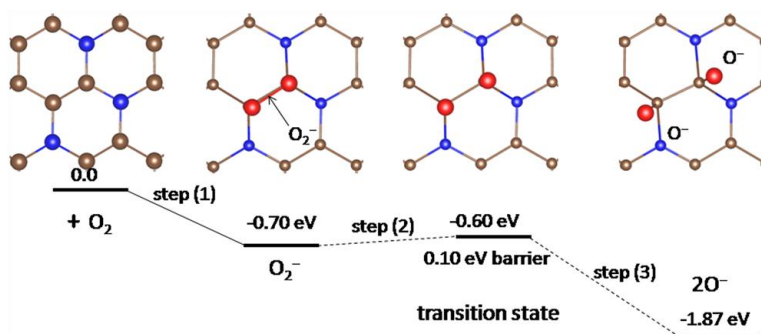


**Figure 4.** The schematic structures of the O<sub>2</sub> dissociation process on the N dopants cluster. Arabic numbers below the arrows in parentheses denoted the reaction steps described in the text. The relative energies in the diagram are taken the total energies of the free O<sub>2</sub> and pristine NG as the energy zero.

Based on the results presented above, the O<sub>2</sub> adsorption and activation process is presented in Fig. 4. Upon the O<sub>2</sub> adsorption, the O<sub>2</sub> molecule gets 0.85 |e| from the carbon dimer in the center of the N dopants, in the form of "O<sub>2</sub><sup>-</sup>", marked as "step (1)"; The "O<sub>2</sub><sup>-</sup>" fragment is dissociated and forms two "O<sup>-</sup>" by further negatively charged by the carbon dimer in the center of the N dopants and other carbon atoms near the N dopants. The calculated energy barrier for the dissociation is 0.10 eV, which is in line with the high activity for the ORR investigated by electrochemical tests presented below.

### 3.2. Structure characterization

XPS analysis indicates that different types of nitrogen species have been in the carbon lattice. XPS survey-scan spectra show the elements for P800-3:1 and P800-xc-72 are composed of carbon, nitrogen and oxygen. Herein, P800-xc-72 denotes the pyrolysis of xc-72 at 800 °C. The determined

atomic percentages of carbon, nitrogen and oxygen for P800-3:1 and P800-xc-72 are 90.16, 5.21, 4.63 and 96.20, 0.23, 3.61, respectively. These results are in good agreement with the data of elemental analysis of both samples. In addition these data indicate the nitrogen content of P800-3:1 is much higher than that of P800-xc-72, so the latter can be negligible.

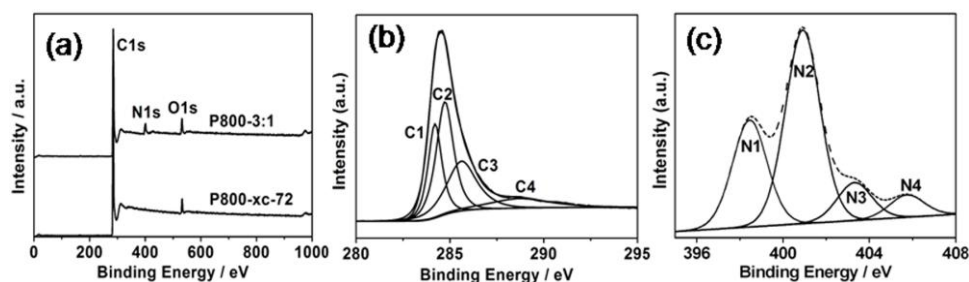


**Figure 5.** XPS (a) survey-scan spectra for P800-xc-72 and P800-3:1; (b) The high-resolution C1s spectrum for P800-3:1; (c) The high-resolution N1s spectrum for P800-3:1.

The increased N of P800-3:1 issues from the pyrrole monomer (C and N) [31]. As displayed by the XPS spectrum in Fig. 5b, for P800-3:1, the major C1s peaks at 284.3 (C1) and 284.7 eV (C2) correspond to  $sp^2$  C in the graphitic domains. The minor peak at 285.6 eV (C3) can be attributed to C-N bonds formed during the heat treatment [32]. The peak at 288.7 eV is assigned to O-C=O [32]. The N 1s spectrum of P800-3:1 (Fig. 5c) could be deconvoluted into three components at 398.4 (N1), 400.9 (N2), 403.3 (N3) and 405.7 eV (N3), corresponding to pyridinic N, graphitic N and oxidized N. It is found that 29.60% N from pyridinic N, 53.72% from graphitic N and 16.68% from oxidized N [33].

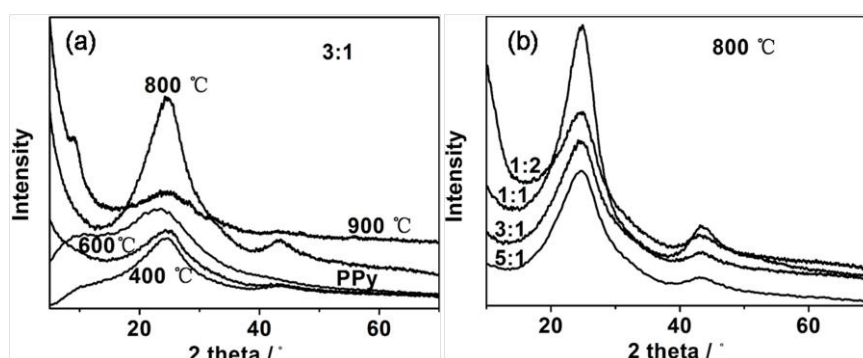


**Figure 6.** XRD patterns (a) untreated PPy and samples obtained by the pyrolysis of PPy/CB (3:1) at different temperatures; and (b) samples prepared at 800 °C with varying PPy to CB weight ratios.

However, the N1s peak of granular PPy mainly appears at 399.6 eV which corresponds to pyrrolic N [34]. It demonstrates that pyrrolic N of PPy is converted to three type nitrogens (i.e. pyridinic N, graphitic N and oxidized N) in the calcination process. The results of XPS and elemental analysis laid the foundation for the structure proposition. For P800-1:2, P800-1:1, P800-3:1 and P800-

5:1, the effective conversion ratio of pyrrolic N to pyridinic N and graphitic N is 13.81%, 15.34%, 26.38% and 7.65%, respectively. It is easy to see P800-3:1 has the highest conversion rate which is consistent with its highest catalytic activity.

XRD analysis has successfully indicated PPy is completely carbonized at 800 °C. The XRD patterns of PPy/CB (3:1) at different pyrolysis temperatures (400 °C, 600 °C, 800 °C and 900 °C) and PPy are presented in Fig. 6a. From Fig. 6a, a peak at 24.5° and a wide peak at 10°-15° are observed for PPy. The similar peaks are also observed for the sample treated at 400 °C. However, the wide peak disappears when the sample is treated at 600 °C, 800 °C or 900 °C. For PPy/CB (3:1), the intensity of the peaks at 24.5° and 43° reach the maximum when the calcination temperature is 800 °C. These observations indicate that the degree of graphitization becomes higher with the increase of calcination temperature. However, the peaks are less intensive when the sample is pyrolyzed at 900 °C. From Fig. 6b, the peaks at 24.5° and 43° which are assigned to the carbon background are observed when the different samples are treated at 800 °C. Referring to Fig. 8b and Fig. 9b which evaluate the effect of different pyrolysis temperatures on the catalytic activity of 3:1, 800 °C is confirmed to be the optimum calcination temperature for PPy.

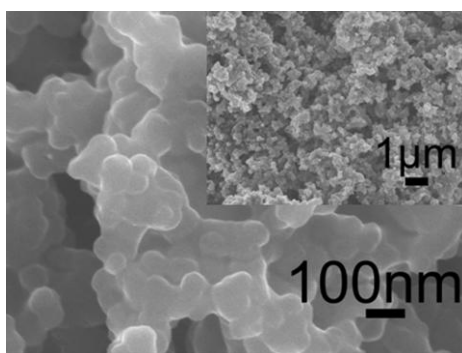


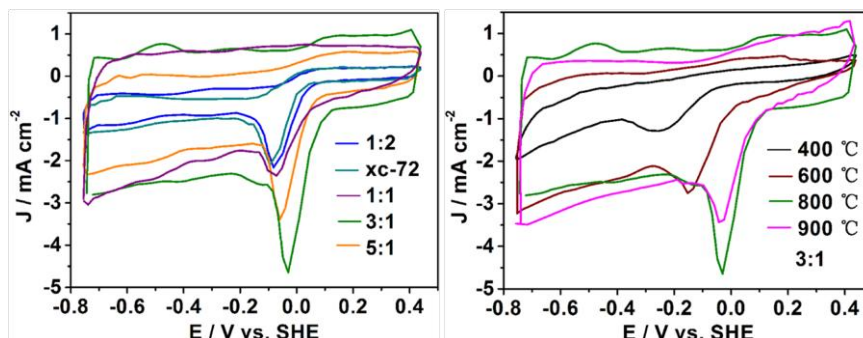
**Figure 7.** FESEM high magnification image of P800-3:1; the inset shows the low magnification image.

As seen in FESEM image (Fig. 7), the structure of P800-3:1 is composed of small particles. Other obtained samples are similar in structure with P800-3:1. There are some holes with different sizes existing in the obtained sample due to irregular accumulation of small particles, which lead to the samples with a little different BET surface area. The BET surface area of P800-1:2, P800-1:1, P800-3:1 and P800-5:1 is 166.4 m<sup>2</sup> g<sup>-1</sup>, 226.9 m<sup>2</sup> g<sup>-1</sup>, 299 m<sup>2</sup> g<sup>-1</sup> and 276.3 m<sup>2</sup> g<sup>-1</sup>, respectively. The differences in BET surface area may also cause them to exhibit slightly different catalytic activities.

### 3.3 Electrochemical activities

The electrocatalytic activities of the synthesized catalysts for ORR were firstly investigated by CV in O<sub>2</sub>-saturated 0.1 M KOH at a scanning rate 50 mV s<sup>-1</sup> and the results were shown in Fig. 8. As shown in Fig. 8a, P800-3:1 shows a higher ORR peak potential (-0.03 V) than P800-xc-72 (-0.10 V).

Moreover, the reduction peak current density for P800-3:1 is almost 2.2 times higher than P800-xc-72 (4.6 and 2.1 mA cm<sup>-2</sup>, respectively). These results clearly indicate that P800-3:1 has better ORR catalytic activity than P800-xc-72.



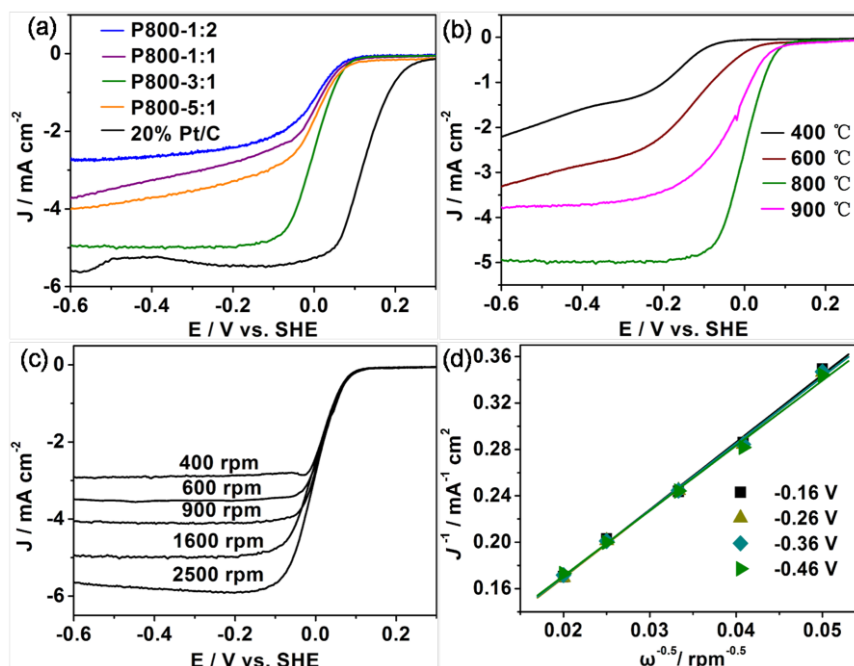
**Figure 8.** Cyclic voltammograms of (a) P800-1:2, P800-xc-72, P800-1:1, P800-3:1 and P800-5:1; (b) P400-3:1, P600-3:1, P800-3:1 and P900-3:1 in an O<sub>2</sub>-saturated 0.1 M KOH solution. Scan rate: 50 mV s<sup>-1</sup>.

Fig. 8a evaluates the effect of PPy loading on the ORR catalytic activities of P800 (1:2, xc-72, 1:1, 3:1 and 5:1). As displayed by Fig. 8a, P800-3:1 has the highest ORR catalytic activity among the synthesized catalysts. As can be seen, the ORR peak potential shifts positively and the oxygen reduction peak current density is gradually elevated with the increase in the amount of PPy. Until polypyrrole to CB weight ratio reaches 3:1, the reduction peak potential gets to the most positive and then begins to shift negatively. Similarly, the reduction current density begins to decrease. In other words, the ORR catalytic activity does not increase with the polypyrrole loading, which differs from the results of previous studies regarding the polymer to CB weight ratios [35].

The impact of different pyrolysis temperature on the catalytic activity of 3:1 is shown in Fig. 8b. The catalytic activity reduces in the order: P800 > P900 > P600 > P400. P800 (-0.03 V, 4.64 mA cm<sup>-2</sup>) shows the most positive ORR peak potential and the highest reduction peak current density than P900 (-0.04 V, 3.43 mA cm<sup>-2</sup>), P600 (-0.15 V, 2.75 mA cm<sup>-2</sup>) and P400 (-0.26 V, 1.29 mA cm<sup>-2</sup>). This is mainly due to the complete decomposition of PPy at 800 °C which results the rearrangements of the chemical structure of PPy and the formation of C-N active sites. The results can also be confirmed by observations of XRD and XPS.

Fig. 9a further investigates the effect of PPy loading on the ORR catalytic activities of P800 (1:2, 1:1, 3:1 and 5:1) by the RDE measurements on a rotating disk electrode for the above samples. It is clear that P800-3:1 is provided with the largest limiting diffusion current with a very wide current plateau. Although the onset potential (0.14 V) and half-wave potential (0.02 V) for the ORR on P800-3:1 modified electrode are still lower than the onset potential (0.22 V) and half-wave potential (0.14 V) for the electrode modified with Pt-C, its limiting diffusion current density is close to that of the Pt-C catalyst. Fig. 9b indicates the onset potential is shifted from -0.1 to 0.14 V when the treating temperature is increased from 400 °C to 800 °C for 3:1. Similarly, the half-wave potential is positively shifted to 0.02 V. However, with a further increase in temperature up to 900 °C, the activity falls

drastically and gives a lower ORR performance. These observations indicate that the optimal treating temperature is around 800 °C.



**Figure 9.** Linear sweep voltammograms (LSVs) for (a) P800-1:2, P800-1:1, P800-3:1, P800-5:1 and 20% Pt/C; (b) P400-3:1, P600-3:1, P800-3:1 and P900-3:1 in an  $O_2$ -saturated 0.1 M KOH solution at a scan rate of  $10 \text{ mV s}^{-1}$  at a rotation speed of 1600 rpm; LSVs for (c) P800-3:1 in an  $O_2$ -saturated 0.1 M KOH solution at a scan rate of  $10 \text{ mV s}^{-1}$  at different rotation speed; Koutecky-Levich plots for (d) P800-3:1 at different electrode potentials. The experimental data were obtained from (c).

The linear sweep voltammetry (LSV) for the ORR was carried out on P800-3:1 modified electrode by changing the rotation speed from 400 to 2500 rpm. Fig. 9c displays the limiting diffusion currents increase along with the rotation speed increasing. For P800-3:1 modified electrode, the limiting diffusion current is observed with a wide current plateau which is similar to Pt-C modified electrode. It implies that the ORR at P800-3:1 modified electrode can likely proceed in an efficient four electron pathway.

The electron transfer number is calculated to be 4.1 on P800-3:1 modified electrode. It is calculated based on the Koutecky-Levich equation [36]. Fig. 9d describes the K-L plots of P800-3:1 at different electrode potentials ranging from -0.6 V to 0.3 V. P800-3:1 shows a good linear relationship between  $J^{-1}$  and  $\omega^{-0.5}$  at the above-mentioned potential. For P800-3:1, the slopes have little change at -0.16 V, -0.26 V, -0.36 V and -0.46 V. It shows that the electron transfer number, which is calculated to be 4.1, is almost the same at different electrode potentials. The results indicate that P800-3:1 is prone to reduce  $O_2$  to  $OH^-$  instead of  $H_2O_2$ . It illustrates that the theoretical calculation is well consistent with the experimental results.

The stability of P800-3:1 was evaluated by cyclic voltammograms and the polarization curves by continuous potential cycling of 1200 cycles in 0.1 M KOH saturated with O<sub>2</sub>. As shown in Fig. 10, after 1200 cycles the oxygen reduction current density only experiences a slight drop and it shows better stability of P800-3:1 in alkaline solution.

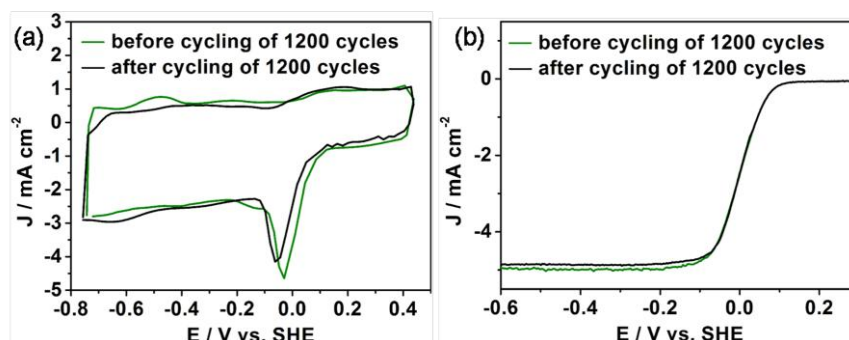


**Figure 10.** (a) Cyclic voltammograms, (b) polarization curves of P800-3:1 in an O<sub>2</sub>-saturated 0.1 M KOH solution before and after potential cycling 1200 cycles. Potential scan rate is 50 mV s<sup>-1</sup> for CV, and 10 mV s<sup>-1</sup> for linear sweep voltammetric curves with the electrode rotating at 1600 rpm.

#### 4. CONCLUSIONS

In summary, metal-free N-doped graphite has been synthesized by the pyrolysis of PPy/CB nanocomposites. The effective conversion rate of nitrogen can be regulated by varying pyrrole to CB weight ratios. P800-3:1 is provided with the highest conversion rate of nitrogen based on XPS analysis. The electrochemical tests on P800-3:1 modified electrode show high electrocatalytic activity and long-term stability for ORR in alkaline media.

The structure of P800-3:1 has been proposed based on DFT calculation and experimental results. The simulation of the O<sub>2</sub> dissociation shows that the carbon dimer in the N-doped center and other carbon atoms around the N doping act together as an electron reservoir in donating electrons for the O<sub>2</sub> adsorption and the cleavage of the O-O bond. The dissociation of O<sub>2</sub> forms two O<sup>-</sup> with very low energy barrier (0.10 eV). The structure of P800-3:1 is proved to be the optimal structure for the ORR according to the consistency of theoretical calculation and the experimental results.

#### ACKNOWLEDGEMENT

This work was supported by the National Natural Science Foundation of China (Grant No. 21171051, 21271066, U1204516, 11147006 and 11174070), the Program for Changjiang Scholars and Innovative Research Team in University (IRT1061), the Innovation Fund for Outstanding Scholar of Henan Province (114200510004), Henan Key Proposed Program for Basic and Frontier Research (112102210005, 112300410095). The simulations were performed on resources provided by the high-performance computing center of College of Physics and Information Engineering in Henan Normal University.

## References

1. C. Wang, H. Daimon, T. Onodera, T. Koda and S. Sun, *Angew. Chem. Int. Ed.*, 47 (2008) 3588.
2. J. Greeley, I.E.L. Stephens, A.S. Bondarenko, T.P. Johansson, H.A. Hansen, T.F. Jaramillo, J. Rossmeisl, I. Chorkendorff and J.K. Nørskov, *Nature Chem.*, 1 (2009) 552.
3. K.A. Kuttiyiel, K. Sasaki, Y.M. Choi, D. Su, P. Liu and R.R. Adzic, *Energy Environ. Sci.*, 5 (2012) 5297.
4. V. Mazumder, M. Chi, K.L. More and S. Sun, *Angew. Chem. Int. Ed.*, 49 (2010) 9368.
5. T. Yang and G. Han, *Int. J. Electrochem. Sci.*, 7 (2012) 10884.
6. G. Wu, K.L. More, C.M. Johnston and P. Zelenay, *Science*, 332 (2011) 443.
7. R.A. Sidik and A.B. Anderson, *J. Phys. Chem. B*, 110 (2006) 1787.
8. C. Arbizzani, S. Righi, F. Soavi and M. Mastragostino, *Int. J. Hydrogen Energy*, 36 (2011) 5038.
9. Z.W. Liu, F. Peng, H.J. Wang, H. Yu, W.X. Zheng and J. Yang, *Angew. Chem. Int. Ed.*, 50 (2011) 3257.
10. Z. Yang, Z. Yao, G. Li, G. Fang, H. Nie, Z. Liu, X. Zhou, X. Chen and S. Huang, *ACS Nano*, 6 (2012) 205.
11. Z.H. Sheng, H.L. Gao, W.J. Bao, F.B. Wang and X.H. Xia, *J. Mater. Chem.*, 22 (2012) 390.
12. K. Gong, F. Du, Z. Xia, M. Durstock and L. Dai, *Science*, 323 (2009) 760.
13. M. Glerup, M. Castignolles, M. Holzinger, G. Hug, A. Loiseau and P. Bernier, *Chem. Commun.*, 41 (2005) 2542.
14. H. Jin, H. Zhang, H. Zhong and J. Zhang, *Energy Environ. Sci.*, 4 (2011) 3389.
15. Y.M. Yu, J.H. Zhang, C.H. Xiao, J.D. Zhong, X.H. Zhang and J.H. Chen, *Fuel Cells*, 12 (2012) 506.
16. S.Y. Yang, K.H. Chang, Y.L. Huang, Y.F. Lee, H.W. Tien, S.M. Li, Y.H. Lee, C.H. Liu, C.C.M. Ma and C.C. Hu, *Electrochem. Commun.*, 14 (2012) 39.
17. I. Y. Jeon, D. Yu, S.Y. Bae, H.J. Choi, D.W. Chang, L. Dai and J.B. Baek, *Chem. Mater.*, 23 (2011) 3987.
18. D. Higgins, Z. Chen and Z. Chen, *Electrochim. Acta.*, 56 (2011) 1570.
19. S. Yang, L. Zhi, K. Tang, X. Feng, J. Maier and K. Müllen, *Adv. Funct. Mater.*, 22 (2012) 3634.
20. L. Feng, Y. Chen and L. Chen, *ACS Nano*, 12 (2012) 9611.
21. C.V. Rao and Y. Ishikawa, *J. Phys. Chem. C*, 116 (2012) 4340.
22. J.P. Perdew, K. Burke and M. Ernzerhof, *Phys. Rev. Lett.*, 77 (1996) 3865.
23. G. Kresse and J. Furthmüller, *Phys. Rev. B*, 54 (1996) 11169.
24. G. Kresse and J. Furthmüller, *Comp. Mater. Sci.*, 6 (1996) 15.
25. G. Kresse and D. Joubert, *Phys. Rev. B*, 59 (1999) 1758.
26. H.J. Monkhorst and J.D. Pack, *Phys. Rev. B*, 13 (1976) 5188.
27. G. Henkelman, A. Arnaldsson and H. Jónsson, *Comput. Mater. Sci.*, 36 (2006) 354.
28. B. Silvi and A. Savin, *Nature*, 371 (1994) 683.
29. S. Ni, Z. Li and J. Yang, *Nanoscale*, 4 (2012) 1184.
30. Y. Feng, F. Li, Z. Hu, X. Luo, L. Zhang, X.F. Zhou, H.T. Wang, J.J. Xu and E.G. Wang, *Phys. Rev. B*, 85 (2012) 1554541.
31. A. Jaramillo, L.D. Spurlock, V. Young and A. Brajter-Toth, *Analyst*, 124 (1999) 1215.
32. C. Hu, Y. Xiao, Y. Zhao, N. Chen, Z. Zhang, M. Cao and L. Qu, *Nanoscale*, 5 (2013) 2726.
33. A. Morozan, P. Jégou, B. Joussetme and S. Palacin, *Phys. Chem. Chem. Phys.*, 13 (2011) 21600.
34. A. Morozan, P. Jégou, S. Campidelli, S. Palacin and B. Joussetme, *Chem. Commun.*, 48 (2012) 4627.
35. W. Xia, J. Masa, M. Bron, W. Schuhmann and M. Muhler, *Electrochem. Commun.*, 13 (2011) 593.
36. S. Wang, D. Yu and L. Dai, *J. Am. Chem. Soc.*, 133 (2011) 5182.